FATIGUE BEHAVIOR OF PSEUDOELASTIC TiNi THIN STRIPS IN AIR AND BODY FLUID SIMULATED ENVIRONMENTS

PETER FILIP[1], KAREL MAZANEC[1]*

This paper is devoted to the fatigue crack propagation behavior of the pseudoelastic TiNi thin strips in air and corrosive environments of simulated body fluids. The objective of this study was to understand the effect of environment on cyclic crack-growth resistance in a 50.6Ni–49.4Ti (at.%) alloy applied for manufacturing of smart medical microdevices. The goal is to provide the necessary data for the life prediction of micro-implant devices employing pseudoelasticity at human body temperature. Characterization of crack growth rates was performed at 37 °C on middle tension (MT) samples in different environments including air, physiological solution (0.9 % NaCl in water), and aerated Hank's solution. Results indicated that the considerable part of recoverable strain was maintained during cyclic loading. The martensitic phase was always detected at the crack tip. Despite the nucleation and growth of martensitic phase on the crack tip during cycling at maximum stress being well below the yield point, TiNi thin strips were found to have a relatively low fatigue crack growth resistance. This behavior contrasts with behavior of bulk TiNi materials reported previously. No significant differences between other metallic materials typically used in medical applications and investigated TiNi alloys were detected.

K e y w o r d s: TiNi shape memory alloys, corrosion fatigue, phase transformation, biomaterials

ÚNAVOVÉ CHOVÁNÍ PSEUDOELASTICKÝCH TENKÝCH PÁSKŮ TiNi VE VZDUCHU A V PROSTŘEDÍ SIMULUJÍCÍM TĚLNOU TEKUTINU

Předložený příspěvek je zaměřen na studium šíření únavové trhliny v pseudoelastických 50,6Ni–49,4Ti (at.%) tenkých páscích zkoušených na vzduchu a v prostředích simulujících tělní tekutiny. Cílem práce bylo pochopit vliv korozního prostředí na růst trhliny u cyklicky zatěžované slitiny TiNi používané pro výrobu inteligentních biomateriálů. Práce poskytuje data potřebná pro predikci životnosti mikroimplantátů využívajících pseudoelastické chování při teplotě lidského těla. Růst únavové trhliny byl sledován na

[1] Institute of Materials Engineering, Faculty of Metallurgy and Materials Engineering, Technical University Ostrava, 17. listopadu 15, 708 33 Ostrava-Poruba, Czech Republic
* corresponding author

MT vzorcích při teplotě 37 °C. Výsledky prokázaly, že značná část vratné deformace byla zachována v průběhu cyklování. Martenzitická fáze byla vždy detekována na čele trhliny. I přesto, že byla pozorována nukleace a růst martenzitu na čele trhliny při cyklování s maximálním tahovým napětím nepřevyšujícím mez kluzu, TiNi tenké pásky vykazovaly poměrně nízkou odolnost vůči růstu únavové trhliny. Toto chování mikromateriálů kontrastuje s dříve popsaným chováním objemných TiNi vzorků. Nebyly detekovány žádné zásadní rozdíly mezi chováním dalších kovových materiálů, typicky využívaných pro medicínské aplikace, a TiNi studovanými materiály.

1. Introduction

Increasing interest in shape memory alloys and particularly in TiNi based intermetallic materials has been accompanied with improving their design and performance [1, 2]. In several fields of medicine, TiNi shape memory alloys have become an attractive replacement for the currently used metallic materials including stainless steel, titanium alloys, and pure titanium [3]. The major advantages related to TiNi applications include the shape memory and the pseudoelasticity, allowing a considerable improvement of biofunctionality of implants, and the superior corrosion resistance of TiNi in physiological environments. Implementing TiNi microdevices, however, requires additional studies pursuing the understanding of their performance in the human body, particularly when long-term applications are required. The surface to volume ratio of microdevices significantly increases when compared to bulk or "macrodevices" currently used. This fact may lead to different behavior when comparing microdevices to bulky materials. Efficient applications of microdevices require understanding of their structural properties involving stress analysis and life prediction. This paper represents one part of a comprehensive research oriented on shape memory phenomena in TiNi alloys and their medical applications [4].

TiNi based alloys with a composition of approximately 50 at.% Ti and 50 at.% Ni exhibit shape memory behavior [5, 6]. The shape memory behavior is a result of a reversible athermal martensitic transformation. Pseudoelastic behavior is observed at temperatures above the austenite finish temperature A_f. At these conditions, the parent high temperature B2 phase transforms into martensite B19' during loading. Since formation of B19' martensite is induced by applied stress, the newly produced B19' phase is called stress-induced martensite (SIM). Upon releasing the applied stress, a reversible transformation of B19' into B2 occurs [1, 5, 6]. Typical stress-strain dependence representing the pseudoelastic behavior of TiNi thin strips is shown in Fig. 1. It can be easily seen from Fig. 1 that three distinct regions characterize the stress-strain behavior. In the first region typified by a large stress increase over a small strain range $\Delta\varepsilon_1$, the elastic deformation of high temperature B2 phase occurs. This purely elastic deformation is followed by the σ-ε dependence plateau with little change in stress over large strain interval $\Delta\varepsilon_2$. The occurrence of plateau is distinguished by a "critical" stress σ_{SIM}, at which

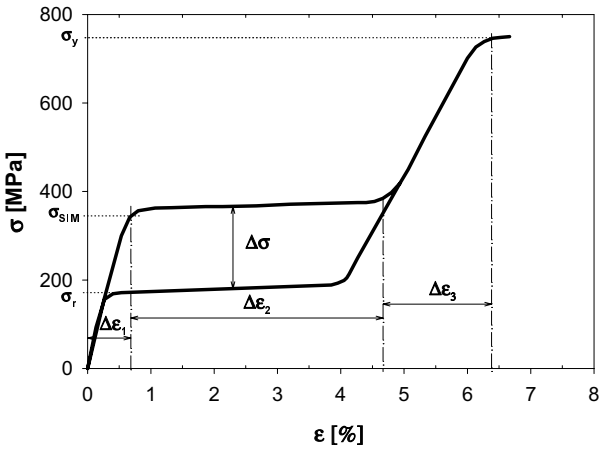

Fig. 1. Characteristic stress-strain dependence of thin TiNi strips, tested at 37 °C.

the martensite B19' phase nucleates and grows [7]. The most compliant martensite variants with respect to the tensile stress axis grow preferentially. After the stress induced B2→B19' phase transformation is completed, elastic deformation of martensite over the strain range $\Delta\varepsilon_3$ occurs until yielding at σ_y. If loading of TiNi is interrupted before reaching σ_y, a completely reversible deformation is observed upon release of applied stress. Elastic unloading of B19' martensite is followed by recoverable phase transformation B19'→B2, at a lower stress σ_r compared to σ_{SIM}, and elastic unloading of B2 parent phase. The maximum recoverable strain and the level of σ_y and σ_{SIM} stresses depend on the structure of TiNi [1, 8]. During cyclic deformation, the characteristic stresses σ_i and strains $\Delta\varepsilon_i$ also vary [1, 8, 9].

It is known that microcracks always exist in materials and fracture mechanics provides a basis for design in the presence of these flaws using damage tolerant concepts. This approach is particularly relevant for human implants. In addition to bulk microcracks, the fabrication of TiNi microdevices invariably leaves a distribution of small cracks on the surface. Although the simple tension and compression properties of TiNi thin strips are reasonably well characterized, there is very little understanding of engineering data on their fracture and cyclic fatigue behavior in a corrosive environment simulating the human body. This information is of major importance as failure of a human implant could result in severe damage. The currently available data describing crack propagation in TiNi alloys under monotonic or cyclic loading are limited to bulk materials [1, 9–12]. Cyclic load and corrosive environment are typical for human implants. Therefore, the design may be limited to the corrosion fatigue threshold ΔK_{th}, which describes the stress intensity range for the onset of crack propagation in a corrosive environment.

Knowing threshold values for pseudoelastic TiNi micron size devices allows estimating the expected lifetime and providing a rational design against fatigue failure in a corrosive environment. The aim of this paper is to describe the fatigue crack propagation behavior of a pseudoelastic TiNi thin layer in simulated physiological environments and to investigate the mechanism of crack growth.

2. Experimental

TiNi material with composition 50.6Ni–49.4Ti (at.%) was received in form of thin strips having dimensions 200 mm × 5 mm × 200 μm. These strips were annealed in an argon atmosphere at 900 ℃ for 60 minutes and subsequently quenched in an ice water bath. A B2 structure with average grain size of 60 μm and without Ti_3Ni_4 precipitate was obtained after this treatment. The content of inclusions TiC, Ti(C,N), $Ti_4Ni_2(O,N)_x$, and Ti_2Ni was 4 vol.%. The maximum size of triangular or hexagonal carbides TiC and carbonitrides Ti(C,N) was 17 μm (average size 13 ± 2 μm). They were detected predominantly at grain boundaries. On the other hand, the $Ti_4Ni_2(O,N)_x$ and Ti_2Ni particles were mostly located within the B2 matrix. $Ti_4Ni_2(O,N)_x$ and Ti_2Ni inclusions exhibited an oval shape with the maximum particle size of 18 μm (average size 12 ± 8 μm).

The tests characterizing the cyclic deformation behavior and the corrosion fatigue tests were performed in this research. Both test types were conducted at 37 ± 1 ℃ in air, physiological solution (0.9 % NaCl in water), and aerated Hank's solution (0.19 g of $CaCl_2 \cdot 2H_2O$, 0.1 g Mg_2SO_4, 0.4 g KCl, 0.06 g anhydrous K_3PO_4, 8 g NaCl, 0.05 g anhydrous Na_3PO_4, 1 g glucose, and 0.35 g $(NaH)CO_3$ per liter of distilled deionized water) having pH of 7. Liquids were forced to circulate by a pump during testing.

The cyclic deformation behavior was investigated by application of 100 uniaxial tensile type loading cycles with the maximum stress approximately 650 MPa and following unloading. During this cycling, the maximum applied strain was 6% (first loading cycle) and the crosshead rate was 1 mm/min. Samples were used in "as received" conditions (no notch present), the clamping distance was 50 mm and the measured length was 25.4 mm.

The corrosion fatigue tests employed standard middle tension (MT) specimens for fatigue crack growth rate testing. Samples with the length $H = 100$ mm, width $W = 5$ mm, and thickness $B = 200$ μm were manufactured by laser cutting from received strips in accordance with ASTM E 647-99 [13]. Cyclic loading (15 Hz sine wave) was applied by use of electro-servo hydraulic machines under automated stress intensity control in general accordance with the testing techniques described in ASTM E647. The clamping distance $2L$ was 20 mm and samples were cycled at a load ratio $R = 0.2$, defined as ratio of minimum to maximum stress intensity factors $R = K_{\min}/K_{\max}$ ($K \approx \sigma\sqrt{a}$, σ being the applied stress and a is the half length of the crack). The crack-growth was monitored optically and the testing

temperature was measured using K-type thermocouples, which were welded to tested TiNi specimens.

TEM experiment was performed using an analytical TEM/STEM microscope Hitachi H7100FA at 100 kV; thin foils were prepared by a careful cutting, dimpling and ion milling.

3. Results and discussion

3.1 Cyclic deformation behavior of TiNi thin strips in corrosive solutions

In the first cycle, TiNi alloy displayed linear elastic deformation until the critical stress for SIM transformation $\sigma_{\mathrm{SIM}} = 378$ MPa, as shown in Fig. 1. The volume fraction of martensite B19' increased during the loading along the plateau and during the following deformation until maximum stress applied. During cycling the maximum applied strain was 6 %. Upon decrease of applied stress, the volume fraction of stress induced martensite decreased. At 195 MPa, the lower stress plateau was detected. The detected stress hysteresis $\Delta\sigma$ is related to energy dissipation during phase transformation. The value of $\Delta\sigma$ strongly depends on the structure of TiNi alloy [1, 5, 6]. After complete unloading, there was no detectable permanent strain and the transformation was pseudoelastic and completely reversible. The detected transformation plasticity related to the upper plateau was approximately 4 % and, when exhausted, the applied stress began to increase again.

Characteristic cyclic behavior, as detected for a uniaxial tensile type loading of TiNi thin strips in a physiological solution at 37 °C, is shown in Fig. 2a. The data including 10^{th}, 50^{th} and 100^{th} cycles of the subsequent cyclic stress strain response

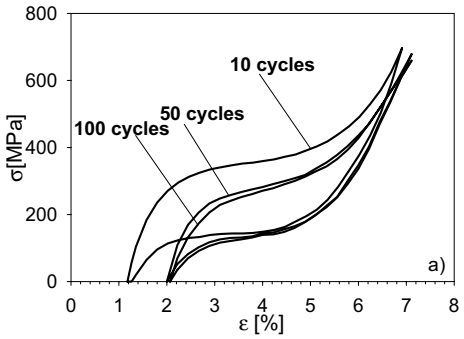

Fig. 2a. Stress-strain dependences detected in 10^{th}, 50^{th} and 100^{th} cycle. Saturation of plastic deformation occurred after 50 cycles.

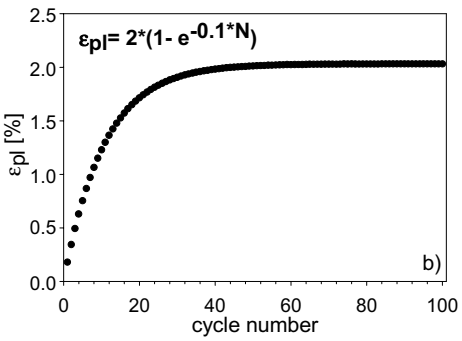

Fig. 2b. Plastic deformation accumulated after cyclic loading.

(strain range $\Delta\varepsilon = 6$ %) indicate that material demonstrated cyclic softening. The stress necessary for nucleation and growth of B19' martensite (σ_{SIM}) decreased with increasing number of cycles in accordance with the data published earlier for macro samples [14]. Accumulation of defects and superposition of generated internal stresses are responsible for this phenomenon [1]. Also the peak stress at the maximum strain decreased with repeated cycling. As apparent from the "shift" of stress-strain dependence, the cyclic loading with $\Delta\varepsilon = 6$ % at 37℃ led to accumulation of permanent plastic deformation $\varepsilon_{\mathrm{pl}}$ despite the fact that the plastic yield point σ_{y} was never reached. Figure 2b shows the extent of $\varepsilon_{\mathrm{pl}}$ strain change with applied number of cycles. It is obvious that the saturation appeared after approximately 50 cycles. This behavior is almost identical with behavior observed in massive (bulky) TiNi materials [13, 14]. After applied 50 cycles, $\varepsilon_{\mathrm{pl}}$ remained relatively constant at a value of 1.8 % and the detected dependence can be approximated by the exponential relationship $\varepsilon_{\mathrm{pl}} = 2 \times (1 - \mathrm{e}^{-0.1N})$, where N is the number of applied cycles. It was shown earlier that the microstructure reached a saturated state, and only insignificant further changes of microstructure occur with continued deformation [1]. A very similar behavior was detected for TiNi samples cyclically loaded in air and aerated Hank's solution at 37℃ and these dependencies are not shown.

3.2 Fatigue crack growth in air and corrosive environments

Results demonstrating the behavior of TiNi thin strips detected in air, physiological solution and Hank's solution are shown in Fig. 3. It can be easily seen from

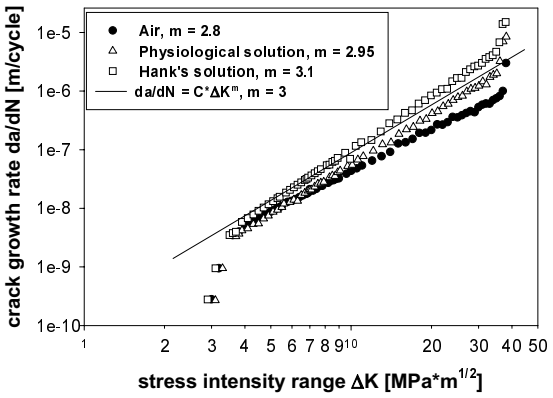

Fig. 3. Fatigue crack growth in investigated TiNi thin strips in three different environments.

comparison of behavior in air and in corrosive liquid solutions simulating body fluids that there was no significant effect of the applied corrosive environment on fatigue behavior at given testing conditions. The detected crack growth rates are almost identical for all three environments employed during testing. This is true despite of the fact that dissolved oxygen in neutral pH solutions and chloride ions in the physiological and Hank's solutions were reported to be corrosive species in fatigue crack growth of metals.

To predict the lifetime of TiNi thin strips, the rate of crack growth was determined from the crack length a versus number of elapsed cycles N. The simplest approach known as Paris-Erdogan power law $\mathrm{d}a/\mathrm{d}N = C\Delta K^m$ can be applied [13], where $\mathrm{d}a/\mathrm{d}N$ is the crack growth rate per cycle, C is a constant, ΔK is the operating stress intensity range, and m is the Paris-Erdogan exponent. This equation is then integrated and the number of cycles until failure N_f is obtained by substituting initial and final crack lengths. For TiNi thin strips, a threshold ΔK_th of 3 MPa$\sqrt{\mathrm{m}}$ was seen with a Paris-Erdogan exponent in the steady state growth regime $m \approx 3$. The stress intensity range at instability prior to failure is approximately $\Delta K \approx 35$ MPa$\sqrt{\mathrm{m}}$.

A typical situation of martensite plate that formed in semi-parallel direction with respect to the crack orientation is shown in Fig. 4. This observation was made with a sample tested in the physiologic solution. Figure 4a is a bright field image, Fig. 4b is the corresponding diffraction pattern and Fig. 4c is the dark field image. It can be easily seen that the elastic stress on the crack tip is effectively eliminated by the formation of B19' martensite. The completed TEM analysis of TiNi also revealed that cracks always progressed in martensitic B19' phase. The typical detected mechanism of crack advancement was bridging of the major crack with small microcracks located in front of the major crack tip. An arrow in Fig. 4a marks the small microcrack in front of the main crack. Analogous mechanism of crack advancement, as described for the sample tested in the physiologic solution and shown in Fig. 4, was observed for all samples tested in three different environments (air and body simulating fluids). Stress induced B2→B19' transformation was always detected in the stretched zone indicating that the maximum stress in the vicinity of the crack tip corresponds to the critical stress σ_SIM, required for the stress induced martensitic phase transformation. Apparently, the B19' martensite forms in spite of the fact that the externally applied macro stress levels are significantly lower than σ_SIM detected in uniaxial tensile experiment. In order to avoid any undesirable influence of thin foil preparation process on the microstructure of investigated materials, seven samples (thin foils) were prepared from tested specimens. The microstructures of these samples were also compared with the microstructure of non-tested (without microcrack) but otherwise identical samples. It was found that TEM observations were reproducible and the foils prepared from non-tested samples (without microcrack) exhibited only the presence of stable B2 phase.

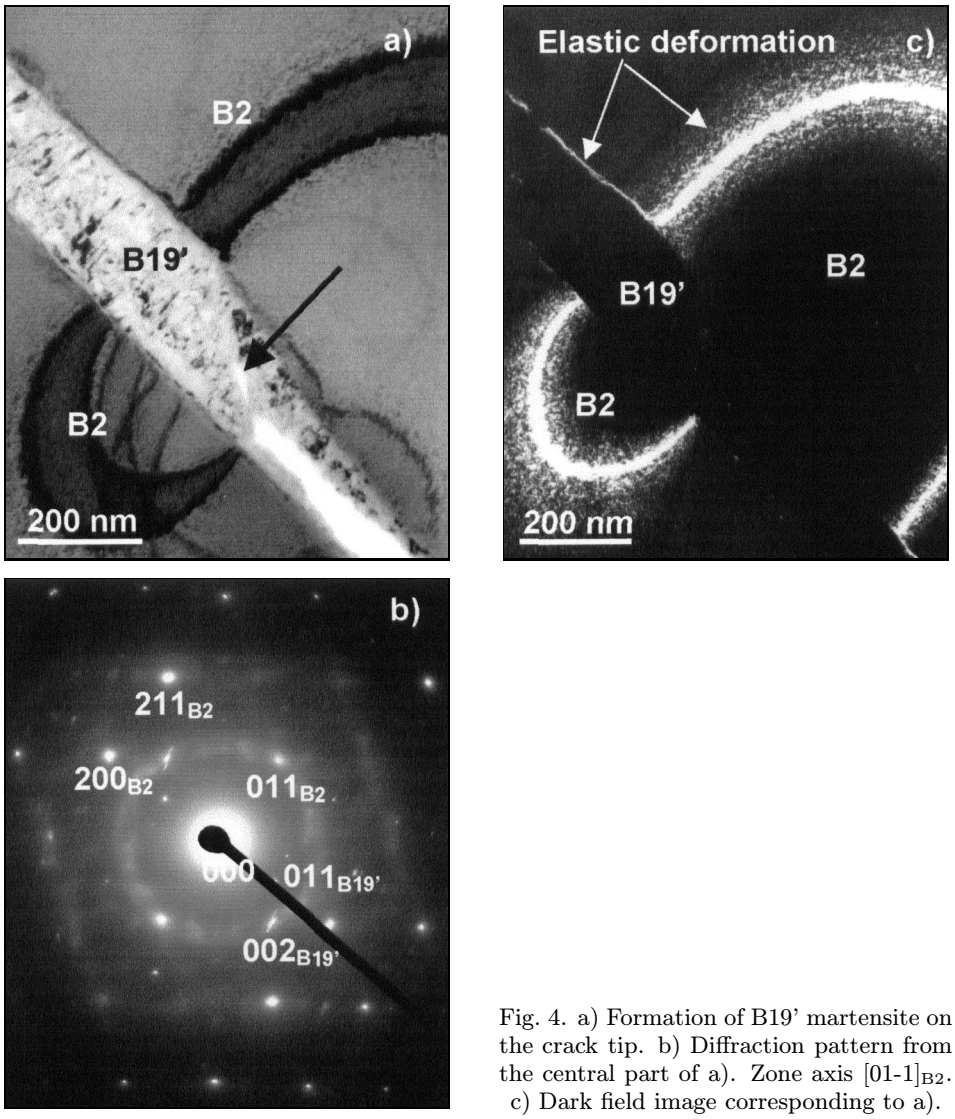

Fig. 4. a) Formation of B19' martensite on the crack tip. b) Diffraction pattern from the central part of a). Zone axis $[01\text{-}1]_{B2}$. c) Dark field image corresponding to a).

The B2→B19' stress induced phase transformation was considered to be a potential source of resistance to fracture and fatigue [1, 9]. Mechanically induced phase transformations have been exploited as methods for increasing the fracture toughness in several materials. Stress induced martensitic transformations are known to occur in austenitic steels and TRIP steels [15, 16]. Transformation toughening was observed also in brittle materials. Phase transformations greatly enhance the fracture toughness of ceramics [17]. In partially stabilized ZrO_2, metastable coherent tetragonal particles are dispersed in a cubic matrix. When a tensile stress

is applied, the metastable tetragonal phase undergoes a martensitic phase transformation to a monoclinic crystal structure. This phase transformation increases the volume of the particles, which reduces the local stress intensity at the crack tip, shielding the tip from the applied load [17, 18]. Studies on the fatigue of austenitic stainless steels and partially stabilized zirconia ceramics have shown that resistance to crack advance can be significantly improved when in situ phase transformation proceeds [17, 18]. However, since in both the stainless steel and zirconia ceramics, the newly formed phase has a larger volume when compared to the parent phase, the transformation involves a positive dilatational component. Due to the elastic constraint of untransformed surrounding material, this results in crack extension into a zone of compressed material. The transformation in TiNi conversely involves largely pure shear with only a small and negative volume change [20], and therefore, it was hypothesized that the micromechanisms contributing to fracture resistance of TiNi are different.

Detailed TEM studies of TiNi thin strips after cyclic loading in different environments revealed that the orientation of B19' martensite plates with respect to crack tip varies between 0 and 45°. This is in accordance with behavior described earlier for the massive steel materials [18]. Obviously a martensite variant, with the most favorable orientation with respect to the stress peak at the advanced crack tip, forms preferentially.

TEM study revealed that the martensitic plates attained their maximum width approximately 200 to 300 nm apart from the advancing crack tip. This distance corresponds to the location of the maximum stress generated in front of the advanced crack during crack opening. It is known that the lateral growth of martensite with respect to the advancing crack strongly depends on the microstructure of the B2 phase. Increased dislocation density constraints the lateral growth of martensitic plates by increasing the B2/B19' interface friction [21]. Conversely, B2 structures with lower dislocation density will allow lateral growth of martensitic plates to a considerably higher extent. This obviously leads to a more pronounced elastic stress relaxation when compared to structures with a higher dislocation density. Systematic observations revealed that after reaching its maximum at the distance 200 to 300 nm apart from the crack tip, the width of B19' martensitic plates slightly decreased. This fact is easily visible in Fig. 4a. However, as apparent from Fig. 4a, the width of the B19' martensitic phase along the major crack significantly decreased (Fig. 4a). Obviously, the unstable B19' martensite transformed back into the B2 phase when the accumulated elastic energy relaxed during formation of new crack surfaces. Pseudoelastic behavior similar to that shown in Fig. 2a occurred in the microvolume adjacent to the advancing crack. The observed retained martensite flanking both sides of the crack (Fig. 4a) was very probably stabilized due to increase of dislocation density occurring during cyclic loading [1, 21]. Clearly, this martensite also contributes to the detected "$\varepsilon_{\mathrm{pl}}$" deformation described above.

Hence the term $\varepsilon_{\mathrm{pl}}$ might represent both the true plasticity and the transformation plasticity related to the stabilized (retained) martensite.

The elastic deformation characterized by the presence of bending contours visible in Fig. 4 was accumulated in both the B2 and B19' phases. As apparent from the dark field image, a very narrow elastically stressed fringes of B2 phase surround the martensitic B19' plate on both sides. This elastic stress evidently forms due to a mismatch between B2/B19' lattices and also as a consequence of the above mentioned negative minor volume change during B2→B19' phase transformation. However, it can be easily seen that the thermoelastic character, accompanied by the formation of semi-coherent B2/B19' interfaces and a low negative volume change related to the B2→B19' phase transformation, significantly limits the accumulation of elastic energy. The thermoelastic character of B2→B19' phase transformation implies that temperature plays a very important role in TiNi alloys. This fact indicates that the physical phenomena in the above-discussed TRIP steels and toughened ceramics differ when compared to TiNi alloys. Hence, the toughening mechanisms are different in TiNi and previously discussed two groups of materials, respectively.

The detected phenomena clearly pointed out that a balance between *i*) the energy related to elastic stress in the bulk, *ii*) the surface energy of the progressing crack, and *iii*) the phase transformation energy is established during cycling behavior and crack growth in TiNi shape memory alloys. Apparently, the energy balance of the thermoelastic phase transformation in TiNi is influenced by the formation of new surfaces (crack growth) and vice versa, the crack growth has an impact on the transformation energy. Since the crack growth represents a conversion of the accumulated elastic energy into the surface energy, the formation and growth of B19' martensite considerably reduces the crack growth potential in TiNi alloys. At a constant temperature, the applied external forces "deliver both energies", hence, the two mentioned processes have a competitive character. The external, mechanically applied energy is partly spent for phase transformation and partly for the formation of new surfaces (crack growth).

TEM analysis revealed that the local critical stress for formation of B19' martensite, σ_{SIM}, is the maximum stress achieved in the vicinity of the crack tip. It is evident that by a proper designing of TiNi transformation temperatures with respect to the application temperature, it is possible to modify the maximum stress on the crack tip and corresponding values of ΔK_{th} and $\mathrm{d}a/\mathrm{d}N$. In accordance with the Clausius-Clapeyron relationship, the σ_{SIM} increases linearly with increasing temperature of TiNi alloys above A_{f} [1, 5]. The amount of transformation energy depends on both the critical stress σ_{SIM} and the transformation plasticity $\varepsilon_{\mathrm{tr}}$ ($E_{\mathrm{T}} \approx \sigma_{\mathrm{SIM}} \times \varepsilon_{\mathrm{tr}}$). In accordance with the Clausius-Clapeyron relationship, the transformation energy varies considerably with temperature. For the constant human body temperature, a TiNi alloy with a lower A_{f} with respect to body tem-

perature (37 ℃) will convert a larger amount of the applied mechanical energy into transformation energy than an alloy with a higher A_f temperature. Hence, the probability of a crack growth will be lower in the alloy with the lower A_f temperature. From an engineering point of view, the difference between the body temperature and A_f should provide a parameter indicating the safety of a TiNi microimplant device.

Also the dislocation density and related capability of B19' martensite to grow laterally with respect to the advancing crack significantly influences the crack growth resistance. Structures with lower dislocation densities allow an easier lateral growth of martensitic plates and related relaxation of elastic energy accumulated as a result of external loading. It was observed that the growth of martensitic plates, which was initiated at the crack tip usually stopped at the high angle grain boundaries or at inclusions present in the microstructure. Hence, a smaller grain size or a higher density of inclusions in a TiNi alloy allow a smaller transformed volume of B19' martensite in front of the advancing crack tip, and a lower consumption of applied energy in the B2→B19' phase transformation, when compared to an alloy with a larger grain size and lower content of inclusions. In general, a higher critical stress σ_{SIM}, a lower dislocation density, a higher metallurgical purity, and a larger grain size of B2 phase will obviously contribute to limitation of the crack growth potential.

The absence of corrosion fatigue in TiNi strips at 15 Hz in physiologic and Hank's solutions, respectively, as well as the persistence of pseudoelastic recovery during cyclic loading is encouraging, however, the threshold values ΔK_{th} are significantly lower compared to other metals and alloys applied currently in medicine. Characteristic threshold value $\Delta K_{th} \approx 4$ MPa$\sqrt{\text{m}}$ was found for Ti-6Al-4V alloy [22], which is a factor of 1.3 greater than the TiNi fatigue threshold. The largest difference in ΔK_{th} when compared to TiNi alloy was detected in commercially pure Ti, which has a fatigue threshold greater than 10 MPa$\sqrt{\text{m}}$ when tested in air at room temperature [23]. Type 316L stainless steel has a $\Delta K_{th} \approx 6$ MPa$\sqrt{\text{m}}$, and the maximum applied stress intensity range prior to failure is nearly 70 MPa$\sqrt{\text{m}}$ [24]. Also a cobalt chrome alloy Haynes 25, which is used in biomedical applications, exhibits a significantly larger threshold value ($\Delta K_{th} \approx 10$ MPa$\sqrt{\text{m}}$ [25]) compared to TiNi alloy. It should be noted, however, that these alloys show a reduction in their threshold in corrosive environments, whereas TiNi is far less susceptible to effect of environment. In contrast to design principles applied for bulk materials, the fatigue crack threshold value becomes increasingly important when microdevices are designed from any materials applicable to human environment. Since the architecture of these devices is very fine, once initiated, the small cracks would readily traverse the entire cross section of a microimplant. It is necessary to design these devices for fatigue resistance based on the threshold ΔK_{th} to prevent crack propagation.

4. Conclusions

TiNi thin strips demonstrated the capacity to undergo a stress induced B2→ →B19' and reverse martensitic transformation after cyclic softening and accumulation of permanent deformation (true plastic deformation and transformation plasticity due to retained martensite) occurred while cyclic testing.

Fatigue crack growth rates in TiNi thin strips at frequency 15 Hz are almost identical in air, physiologic 0.9 NaCl solution, and aerated Hank's solution, respectively. Also threshold ΔK_{th} for the onset of fatigue crack growth ($\Delta K_{\mathrm{th}} \approx 3$ MPa$\sqrt{\mathrm{m}}$), Paris-Erdogan exponents ($m \approx 3$), and the maximum applied ΔK at instability prior to failure ($\approx$ 35 MPa$\sqrt{\mathrm{m}}$) were found to be equal for all three environments.

Stress induced B2→B19' transformation was always detected at the crack tip indicating that the maximum stress in the vicinity of the crack tip corresponds to the critical stress σ_{SIM}, required for the stress induced martensitic phase transformation. The crack growth occurred in martensitic B19' phase. This was detected for all three environments.

When compared to other biomedical metallic materials, the fatigue crack growth resistance of TiNi thin strips was lower. Specifically, the fatigue threshold value ΔK_{th} was considerably less by factor between 1.3 and 3.3 than stainless steel 316L, pure Ti, Ti-6Al-4V alloy, and CoCr Haynes 25 alloy. These parameters can be improved by designing proper transformation temperatures with respect to application temperature of pseudoelastic TiNi devices, controlling the B2 grain size, dislocation density, and metallurgical purity of TiNi alloys.

Acknowledgements

This research was supported by the Ministry of Education of the Czech Republic (project LN 00 B029). The paper is dedicated to Professor Ing. Dr. Vladimír Sedláček, DrSc., on the occasion of his 80th birthday.

REFERENCES

[1] FILIP, P.: Trans. TU Ostrava, Metallurgical Series XLV, 1999, No. 1, p. 1.
[2] VAN HUMBEECK, J.: Mater. Sci. Eng., *A273–275,* 1999, p. 134.
[3] FILIP, P.: Titanium–Nickel Shape Memory Alloys in Medical Applications. In: Titanium in Medicine. Eds.: Brunette, D. M. et al. Berlin, Heidelberg, New York, Springer Verlag 2001, p. 86.
[4] FILIP, P.—MAZANEC, K.: Kovove Mater., *39,* 2001, p. 31.
[5] WAYMAN, C. M.: Shape Memory and Related Phenomena, Progr. Mater. Sci., *36,* 1992, p. 203.
[6] OTSUKA, K.—WAYMAN, C. M.: Shape Memory Materials. Cambridge University Press 1998.
[7] OTSUKA, K.—REN, X.: Mater. Sci. Eng., *A273–275,* 1999, p. 89.
[8] FILIP, P.—MAZANEC, K.: Scr. Met. Mater., *32,* 1995, p. 1375.

[9] FREMOND, M.—MYIAZAKI, S.: Development of Shape Memory Alloys. Wien, New York, Springer Verlag 1996.
[10] MELTON, K. N.—MERCIER, O.: Acta Metall., *27,* 1979, p. 137.
[11] DAUSKARDT, R. H.—DUERIG, T. W.—RITCHIE, R. O.: In: Proceedings of MRS International Meeting on Advanced Materials. Eds.: Otsuka, K., Shimizu, K. Vol. 9. Pittsburgh, MRS 1989, p. 243.
[12] MYIAZAKI, S.—SUIZU, M.—OTSUKA, K.—TAKASHIMA, T.: In: Proceedings of MRS International Meeting on Advanced Materials. Eds.: Otsuka, K., Shimizu, K. Vol. 9. Pittsburgh, MRS 1989, p. 263.
[13] ASTM-E 647 Standard Test Method for Measurement of Fatigue Crack Growth Rates. USA 1999.
[14] FILIP, P.—LAZAR, V.—MAZANEC, K.: In: III. International Conference Fatigue and Degradation of Material Properties. Eds.: Skočovský, P. et al. Vol. 1. Žilina, DT Žilina 1993, p. 5.
[15] STRINGFELLOW, R. G.—PARKS, D. M.—OLSON, G. B.: Acta Metall. Mater., *40,* 1992, p. 1703.
[16] JACQUES, P.—LADRIERE, J.—DELANNAY, F.: Metall. Mater. Trans., *32A,* 2001, p. 2759.
[17] BECHER, P. F.: Acta Metall., *34,* 1986, p. 1885.
[18] DAUSKARDT, R. H.—YU, W.—RITCHIE, R. O.: Jnl. Amer. Ceram. Soc., *70,* 1987, p. 248.
[19] MAGEE, C. L.—PAXTON, H. W.: Trans. TMS – AIME, *242,* 1968, p. 1741.
[20] FILIP, P.: Physical metallurgy parameters of shape memory phenomena in TiNi alloys and possibilities of their practical applications. [Ph. D. thesis]. FMMI – TU Ostrava 1988 (in Czech).
[21] FILIP P.—MAZANEC, K.: Scr. Mater., *35,* 1996, p. 349.
[22] SHIMOJO, M.—HIGO, Y.—OYA-SEIMIYA, Y.: Metall. Mater. Trans., *31A,* 2000, p. 1435.
[23] RITCHIE, R. O. et al.: Internat. Jnl. Fatigue, *21,* 1999, p. 653.
[24] PICKARD, A. C.—RITCHIE, R. O.—KNOTT, J. F.: Met. Technol., *2,* 1975, p. 253.
[25] RITCHIE, R. O.—LUBOCK, P.: Jnl. Biomed. Eng., *108,* 1986, p. 153.

Received: 12.7.2002
Revised: 17.12.2002